04/03/2025 01:15

(Article begins on next page)

Speed Sensor Fault Tolerant PMSM Machines: From Position-Sensorless to Sensorless Control

C.M. Verrelli, S. Bifaretti, E. Carfagna, A. Lidozzi, L. Solero, F. Crescimbini, M. Di Benedetto

Abstract— **New sensorless observers (i.e., from stator currents/voltages measurements), to be included into a simple observer-based sensorless control for the tracking of non-definitely zero speed references in nonsalient-pole surface Permanent Magnet Synchronous Machines (PMSMs), are proposed. They are obtained, through a 'minimum distance' modification, from recently presented position-sensorless observers (i.e., from rotor speed and stator currents/voltages measurements). The rotor speed estimate is here directly provided by the Phase Locked Loop (PLL)-based third-order Steady-State Linear Kalman Filter (SSLKF) that has been previously used to mitigate the distortions on the estimated position. Experimental results illustrate the effectiveness of the proposed approach in a speed sensor fault-tolerant scenario.**

Index Terms— **Permanent magnet synchronous machines; position-sensorless control; sensorless control; observer-based control; speed sensor fault tolerance.**

I. INTRODUCTION

Different control solutions for PMSMs have been proposed in the literature. The reader is referred to: i) [1], [2], [3], [4], [5], [6], [7] for the case in which mechanical variables (rotor position/speed) are measured (see also [8], [9], [10], [11] for synchronization problems and [12], [13] for extensions to PM stepper motors); ii) [14], [15], [16], [17], [18], [19], [20], [21], [22], [23], [24], [25] for recent theoretical/experimental results on sensorless control (see also [26], [27], [28], [29]).

Recently, new design ideas have been presented in [30] (see also [31] for theoretical foundations, as well as for the extension to the case of definitely zero speed references and uncertain stator resistance), showing that, in order to successfully address the position-sensorless case in which the rotor speed ω is available for feedback [for instance, measured through a low-resolution transducer only providing a single pulse per revolution (1 ppr)], it is possible: i) to specialize the design steps of the 'sensorless' observer in [24] (see also [32]), leading to Observer I of [30]; ii) to follow the design ideas presented in [33] (according to the letter swap in [25]), leading to Observer II of [30]. The rotor position still remains unmeasured, with no open loop integration of the rotor speed signal from known initial conditions being allowed to be performed. It is in fact well-known that *non-robust open loop* integration of the rotor speed signal from *'somehow known'* initial conditions

C.M. Verrelli and E. Carfagna are with the Electronic Engineering Department, University of Rome Tor Vergata, Via del Politecnico 1, 00133 Roma, Italy. S. Bifaretti (corresponding author) is with the Industrial Engineering Department, University of Rome Tor Vergata, Via del Politecnico 1, 00133 Roma, Italy, (e-mail: bifaretti@ing.uniroma2.it). A. Lidozzi, L. Solero, F. Crescimbini, and M. Di Benedetto are with the Engineering Department, ROMA TRE University, Via della Vasca Navale 79, 00146 Roma, Italy.

leads, in the presence of noise measurements, to several implementation issues. In contrast to the main contribution of [31] (Section 5), no information, in [30], about the crucial signals $\cos(p\theta)$ and $\sin(p\theta)$ [$p\theta$ is the electrical angle] is directly extracted from the speed dynamics. As aforementioned, the speed measurement is in fact there assumed to be provided by a low-resolution sensor that does not provide sufficiently precise information on the rotor speed. This makes the persistency of excitation condition $\mathcal{P}$:

there exist positive reals T and c_p such that

$$\mathcal{P}: \quad \int_t^{t+T} \omega(\tau)^2 \mathrm{d}\tau \quad \geq \quad c_p, \quad \forall\, t \geq 0$$

is satisfied,

crucial in the estimation process (see in particular Remark 5 in [24] and the related discussion in [31]; the reader is also referred to [34] for the related Persistency of Excitation Lemma). While estimation cannot be achieved for definitely zero rotor speeds[1], estimation is actually guaranteed in the case of non-definitely zero rotor speeds. Applications include PMSM-based generating units, with active/reactive power control goals (see for instance [35]) being out of the scope of this paper. For the sake of clarity, Figure 1 shows the overall observer-based position-sensorless control scheme suggested in [30] (relying on either Observer I or Observer II). The rotor speed measurement is provided by the low-resolution (1 ppr) transducer, whereas the PLL-SSLKF of [36] (see Figure 2 and also [37] for the related (almost constant-rotor-acceleration) approximations) is employed to mitigate the estimated angle distortions. Such a technique (see also [38]) allows in fact to obtain clean signals without introducing significant lags. This structure has been also employed to reduce the speed measurement noise in drives using an electromagnetic resolver ([39]) or an incremental encoder ([40]) or to obtain an estimation of the phasor angle in polluted grids ([36]) leading to an accurate tracking of the input signals even in critical conditions.

In this paper, differently from other related sensorless approaches in the literature (the reader is referred to the recent [41], [42] and references therein and also to [43], [44],[45]),

---

[1]If the information about $\sin(p\theta)$ and $\cos(p\theta)$ is directly extracted from the speed dynamics (with a slight modification of the observer design), then the requirement of a non-definitely zero speed can be avoided (see [31]). However, a new persistency of excitation condition will result: it relies on a non-constant i_d and may affect the machine power losses (see [31]).
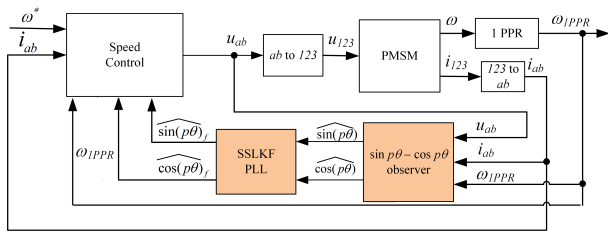
Fig. 1. Block scheme for the position-sensorless control strategy that is based on either Observer I or Observer II in [30] as sin(pθ)-cos(pθ) observer block.
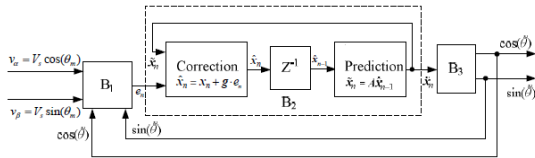

Fig. 2. PLL-SSLKF in [36]: block B1) $e_n \approx \sin(e_n) = \sin(\theta_m - \tilde{\theta}) = V_s^{-1}(v_\beta \cos(\tilde{\theta}) - v_\alpha \sin(\tilde{\theta}))$; B3) numerical procedure or look-up-table to compute $\cos(\tilde{\theta})$, $\sin(\tilde{\theta})$ from $\tilde{\theta}$. Here: V_s is replaced by 1; $\cos(\tilde{\theta})$, $\sin(\tilde{\theta})$ are replaced by $\widehat{\cos(p\theta)}_f$, $\widehat{\sin(p\theta)}_f$; $\cos(\theta_m)$, $\sin(\theta_m)$ are replaced by $\widehat{\cos(p\theta)}$, $\widehat{\sin(p\theta)}$.

we answer the following question: how can the control scheme of [30] (namely, Figure 1) be adapted, through a 'minimum distance' modification, in the case of speed sensor faults? This is a relevant issue, since 'smooth' transitions from speed measurement-based controls to sensorless controls are to be guaranteed in speed sensor fault scenarios. In this respect, speed/position sensors are typically used in speed-controlled electric motors. They can present faulty or uncorrect operations: intermittent sensor connection, DC bias in sensor measurements or sensor gain drop. The most severe fault is, however, the complete sensor outage, which implies a complete lack of speed information and may lead to closed loop instability, especially when it is not quickly recognized and no proper action is performed. The reader is referred to the recent [46] and [47] for very recent related contributions and for an exhaustive review on fault detection in electrical machines, respectively; see also [48], [49], [50], [51] (and references therein) for more general kinds of faults, as well as [52], [53], [54], [55], [56] and [57], [58], [59], [60], [61] for related observer-based applications. On the other hand, fault tolerance is particularly advantageous in electric vehicles applications (see again [41]), in which operation continuity is a key feature (see [57], [54], [62], [63] and [64], [65], [66], [56], [67], [68], [69]), with safety playing a crucial role.

The key-idea of this paper (see [70] for preliminary results) does not rely on coming back to the (more complex) theoretically-based sensorless control of [24] but, rather, on using the PLL-SSLKF of Figure 1 to even obtain a speed estimate, namely $\hat{\omega}$, and thus to replace the position-sensorless scheme of [30] by the a new sensorless scheme, namely the one reported in Figure 3. The PLL-SSLKF block processes the estimates of the unmeasured sinusoidal function of the

electrical angle. They are, in turn, provided by the modified electrical position-observers Observers I and II, in which the measured speed is now replaced by the estimated one. The effectiveness of such an approach is illustrated in Section VII by experimental results concerning a speed sensor fault-tolerant scenario.
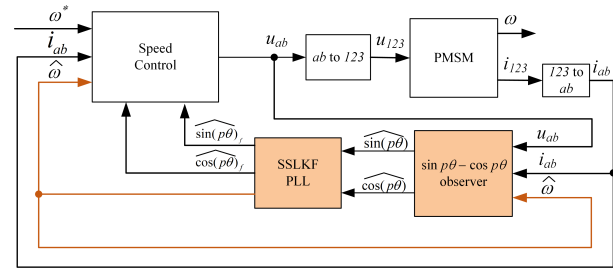

Fig. 3. Block scheme for the new sensorless control strategy.

II. PMSM MODEL

Assume no saliency and restrict the analysis to the sinusoidal flux density distribution. The dynamics of a PMSM in the fixed reference frame are thus given by the fourth order model in [2], [6]:

$$
\begin{aligned}
\dot{\theta} &= \omega \\
\dot{\omega} &= \frac{k_M}{J}\left[-i_a \sin(p\theta) + i_b \cos(p\theta)\right] - \frac{T_L}{J} \\
\frac{di_a}{dt} &= -\frac{R}{L}i_a + \frac{k_M}{L}\omega \sin(p\theta) + \frac{u_a}{L} \\
\frac{di_b}{dt} &= -\frac{R}{L}i_b - \frac{k_M}{L}\omega \cos(p\theta) + \frac{u_b}{L},
\end{aligned}
\tag{1}
$$

where θ is the rotor angle, ω is the rotor speed, (i_a, i_b) are the stator currents, (u_a, u_b) are the stator voltages. The variables $(\theta, \omega, i_a, i_b)$ constitute the states of the system, while (u_a, u_b) represent the control inputs. The effect of the viscous friction coefficient F, which is assumed to be constant and known in [24], is here neglected. Generalizations to the case of non-zero known viscous friction coefficient turn to be straightforward. The load torque T_L is unknown since it depends on applications, while the known machine (positive) parameters are: number of pole pairs p, moment of inertia J, stator windings resistance R, stator windings inductance L, torque constant $k_M = p\Phi_{PM}$ with Φ_{PM} being the permanent magnets flux linkage. The stator fluxes (ξ_a, ξ_b) satisfy the relationships in [6] (see [31]):

$$
\begin{aligned}
\xi_a &= Li_a + \frac{k_M}{p}\cos(p\theta) &\doteq Li_a + \Pi_c \\
\xi_b &= Li_b + \frac{k_M}{p}\sin(p\theta) &\doteq Li_b + \Pi_s.
\end{aligned}
\tag{2}
$$

Here, the quantities

$$
\begin{aligned}
\Pi_c &= \frac{k_M}{p}\cos(p\theta) &= \Phi_{PM}\cos(p\theta) \\
\Pi_s &= \frac{k_M}{p}\sin(p\theta) &= \Phi_{PM}\sin(p\theta)
\end{aligned}
\tag{3}
$$

represent the contributions of the permanent magnets to the stator flux generation. Introduce the Park's transformation, that is the transformation of the vectors $u = [u_a, u_b]^T$ and $i = [i_a, i_b]^T$ in the fixed stator frame (a, b) into vectors expressed in the frame (d, q) rotating along the fictitious excitation current i_f directed as the d axis:

$$\begin{bmatrix} w_d \\ w_q \end{bmatrix} = \mathcal{R}(p\theta) \begin{bmatrix} w_a \\ w_b \end{bmatrix} \qquad (4)$$

$$\mathcal{R}(p\theta) = \begin{bmatrix} \cos(p\theta) & \sin(p\theta) \\ -\sin(p\theta) & \cos(p\theta) \end{bmatrix}.$$

The dynamics (1) expressed in terms of currents and voltages in rotating (d, q) coordinates then become

$$\begin{aligned} \dot{\theta} &= \omega \\ \dot{\omega} &= \frac{k_M}{J} i_q - \frac{T_L}{J} \\ \frac{di_d}{dt} &= -\frac{R}{L} i_d + p\omega i_q + \frac{u_d}{L} \\ \frac{di_q}{dt} &= -\frac{R}{L} i_q - p\omega i_d - \frac{k_M}{L} \omega + \frac{u_q}{L}. \end{aligned} \qquad (5)$$

III. OBSERVER-BASED SPEED CONTROL

Model (5) is suitable for control design. The rotor speed dynamics in the (d, q)-coordinates are, as for DC machines, linear with respect to the stator current vector q-component i_q and can be controlled by it, with the stator current vector d-component i_d being freely assignable to match additional control requirements. Adaptive back-stepping techniques can be successfully applied to design the stator current loops for rotor speed tracking/regulation purposes, provided that a suitable closed loop adaptive observer for the unmeasured quantities is designed. To this purpose, let us denote by the $\mathcal{P}$-signal $\omega^*(t)$ the (non definitely zero) smooth bounded reference signal for the rotor speed $\omega(t)$, with bounded time derivatives $\dot{\omega}^*(t)$ and $\ddot{\omega}^*(t)$. Let us also denote by $i_d^*(t)$ a suitable smooth bounded reference signal with bounded time derivatives for the stator current vector d-component (it will be assumed to be zero in the experimental set-up of Section VI). We report a simplified version of the (theoretically derived and experimentally tested) 'sensorless' control in [24]:

$$\begin{bmatrix} u_a \\ u_b \end{bmatrix} = \begin{bmatrix} \widehat{\cos(p\theta)}_f & -\widehat{\sin(p\theta)}_f \\ \widehat{\sin(p\theta)}_f & \widehat{\cos(p\theta)}_f \end{bmatrix} \begin{bmatrix} u_d \\ u_q \end{bmatrix}$$

$$u_d = L\Big[-\phi_d - k_i(i_d - i_d^*)$$
$$-k_{iI} \int_0^{\cdot} (i_d - i_d^*)\mathrm{d}\cdot\Big]$$

$$u_q = L\Big[-\phi_q - k_i(i_q - i_q^*)$$
$$-k_{iI} \int_0^{\cdot} (i_q - i_q^*)\mathrm{d}\cdot\Big]$$

$$\phi_d = p\hat{\omega} i_q \qquad (6)$$

$$\phi_q = -p\hat{\omega} i_d - \frac{k_M}{L}\hat{\omega}$$

$$\begin{bmatrix} i_d \\ i_q \end{bmatrix} = \begin{bmatrix} \widehat{\cos(p\theta)}_f & \widehat{\sin(p\theta)}_f \\ -\widehat{\sin(p\theta)}_f & \widehat{\cos(p\theta)}_f \end{bmatrix} \begin{bmatrix} i_a \\ i_b \end{bmatrix}$$

$$i_q^* = -k_\omega(\hat{\omega} - \omega^*) - k_{\omega I} \int_0^{\cdot} (\hat{\omega} - \omega^*)\mathrm{d}\cdot.$$

It can be interpreted as an observer-based modification of the classical field-oriented control (with preliminary nonlinear compensation). It depends on the positive control parameters k_i, k_{iI}, k_ω, $k_{\omega I}$ and on the estimates $(\widehat{\sin(p\theta)}_f, \widehat{\cos(p\theta)}_f)$, $\hat{\omega}$ for the quantities $(\sin(p\theta), \cos(p\theta))$, ω. Such estimates are provided in this paper by the new 'sensorless' PLL-SSLKF and observer blocks of Figure 3, which incorporate the modifications of either Observer I or Observer II in [30] [with the measured speed being replaced by the estimated one].

IV. POSITION OBSERVERS WITH MEASURED SPEED

In this section we report, for the sake of clarity, the two theoretically-based observers presented in [30] (see [31] for rigorous stability proofs, in the more general case of uncertain stator resistance) that resort to the use of the speed measurements. According to stability proof of [31], the observers of this section rely on $\mathcal{P}$, i.e., on the requirement of a non-definitely zero ω that becomes a non-definitely zero speed reference ω^* when the observers are included in the observer-based control of the previous section (with a local nature being consequently inherited by the overall error system in accordance with Lemma 9.2 in [71]).

A. Observer I in [30]

The idea underlying the ω- adaptive observer in [24] (and [23]) was to take advantage from the triangularity structure in the (i_q, ω)-subsystem. When the rotor speed is measured, the information about (ξ_a, ξ_b) (and thus about $\cos(p\theta), \sin(p\theta)$) can be fully taken, with stability arguments similar to the ones adopted in [24], from (i_d, i_q) [or equivalently from (i_a, i_b)]. The $(\hat{\xi}_a, \hat{\xi}_b)$-estimation laws in [24] and [27] are thus generalized by (γ_1, along with k_e, γ_θ, are positive design parameters, $\tilde{i}_a = i_a - \hat{i}_a$, $\tilde{i}_b = i_b - \hat{i}_b$)

$$\begin{aligned} \dot{\hat{i}}_a &= -\frac{R}{L}\hat{i}_a + \frac{k_M}{L}\omega\widehat{\sin(p\theta)} + \frac{u_a}{L} + k_e\tilde{i}_a \\ \dot{\hat{i}}_b &= -\frac{R}{L}\hat{i}_b - \frac{k_M}{L}\omega\widehat{\cos(p\theta)} + \frac{u_b}{L} + k_e\tilde{i}_b \\ \dot{\hat{\xi}}_a &= -Ri_a + u_a + \gamma_\theta\Big(\hat{\xi}_a - Li_a\Big)\mathcal{F} - \frac{p\omega}{L\gamma_1}\tilde{i}_b \\ \dot{\hat{\xi}}_b &= -Ri_b + u_b + \gamma_\theta\Big(\hat{\xi}_b - Li_b\Big)\mathcal{F} + \frac{p\omega}{L\gamma_1}\tilde{i}_a, \quad (7) \end{aligned}$$

where, according to [24],

$$\begin{aligned} \mathcal{F} &= \frac{k_M^2}{p^2}\Big[1 - \widehat{\cos(p\theta)}^2 - \widehat{\sin(p\theta)}^2\Big] \\ \widehat{\cos(p\theta)} &= \frac{p}{k_M}\Big(\hat{\xi}_a - Li_a\Big) \\ \widehat{\sin(p\theta)} &= \frac{p}{k_M}\Big(\hat{\xi}_b - Li_b\Big). \end{aligned} \qquad (8)$$

The crucial role of the feedback injection is played by $\mathcal{F}$, which is related to the $\sin(p\theta)$ and $\cos(p\theta)$ estimation errors, in accordance with

$$\begin{aligned} 1 - \widehat{\cos(p\theta)}^2 - \widehat{\sin(p\theta)}^2 &= \cos(p\theta)^2 + \sin(p\theta)^2 \\ &\quad - \widehat{\cos(p\theta)}^2 - \widehat{\sin(p\theta)}^2. \end{aligned}$$

B. Observer II in [30]

The adaptive $(\cos(p\theta), \sin(p\theta))$-observer of the previous subsection is structurally local due to the $\mathcal{F}$-term injection. A global $(\cos(p\theta), \sin(p\theta))$ adaptive observer can be actually obtained by following the design ideas that are presented in the first part of the control design in [33] and are related to a suitable change of coordinates for the error system under persistency of excitation. To this purpose, a part of the PMSM dynamics is to be rewritten as a state space system with state variables i_a, i_b, $\cos(p\theta)$, $\sin(p\theta)$ and the unmeasured quantities $\sin(p\theta)$ and $\cos(p\theta)$ are to be viewed as uncertain 'parameters' to be estimated. The adaptive observer then reads:

$$
\begin{aligned}
\frac{d\hat{i}_a}{dt} &= -\frac{R}{L}i_a + \frac{k_M}{L}\omega\widehat{\sin(p\theta)} + \frac{u_a}{L} + k_i(i_a - \hat{i}_a) \\
\frac{d\hat{i}_b}{dt} &= -\frac{R}{L}i_b - \frac{k_M}{L}\omega\widehat{\cos(p\theta)} + \frac{u_b}{L} + k_i(i_b - \hat{i}_b) \\
\frac{d\widehat{\cos(p\theta)}}{dt} &= -p\omega\widehat{\sin(p\theta)} + v_c \\
\frac{d\widehat{\sin(p\theta)}}{dt} &= p\omega\widehat{\cos(p\theta)} + v_s,
\end{aligned}
\tag{9}
$$

in which k_i is a positive design parameter, while v_s, v_c are chosen as (k_E is a positive design parameter):

$$
\begin{aligned}
v_c &= -k_E\omega(i_b - \hat{i}_b) \\
v_s &= k_E\omega(i_a - \hat{i}_a).
\end{aligned}
\tag{10}
$$

They are related to the regressor matrix

$$
\Gamma = \begin{bmatrix} 0 & \frac{k_M}{L}\omega \\ -\frac{k_M}{L}\omega & 0 \end{bmatrix}.
$$

The observer of this subsection, in contrast to the one reported in the previous subsection, is a purely adaptive, back-EMF- based observer. It can be obtained from Observer I by: computing the dynamics of $\widehat{\cos(p\theta)}$, $\widehat{\sin(p\theta)}$ in (8) for $\gamma_\theta = 0$, $\delta_s = 1$ $\gamma_1 = p^2/(k_M L k_E)$; taking k_i in place of k_e; replacing $\hat{i}_a$, $\hat{i}_b$ by i_a, i_b (respectively) in the first terms appearing in the stator current estimation laws; replacing i_a, i_b by $\hat{i}_a$, $\hat{i}_b$ (respectively) in the last two equations of (8); adding the proportional terms $Lk_i\tilde{i}_a$ and $Lk_i\tilde{i}_b$ to the $(\hat{\xi}_a, \hat{\xi}_b)$-dynamics (respectively).

V. New sensorless position observers

The paper contribution relies on replacing the rotor speed measurement in the previous observers I and II by the output $\hat{\omega}$ of the PLL-SSLKF block of Figure 3, in order to naturally define a new sensorless speed control for (nonsalient-pole surface) PMSMs.

A. Modified observer I

The resulting modified Observer I reads (γ_1, along with k_e, γ_θ, are positive design parameters, $\tilde{i}_a = i_a - \hat{i}_a$, $\tilde{i}_b = i_b - \hat{i}_b$):

$$
\begin{aligned}
\dot{\hat{i}}_a &= -\frac{R}{L}\hat{i}_a + \frac{k_M}{L}\hat{\omega}\widehat{\sin(p\theta)} + \frac{u_a}{L} + k_e\tilde{i}_a \\
\dot{\hat{i}}_b &= -\frac{R}{L}\hat{i}_b - \frac{k_M}{L}\hat{\omega}\widehat{\cos(p\theta)} + \frac{u_b}{L} + k_e\tilde{i}_b \\
\dot{\hat{\xi}}_a &= -Ri_a + u_a + \gamma_\theta\left(\hat{\xi}_a - Li_a\right)\mathcal{F} - \frac{p\hat{\omega}}{L\gamma_1}\tilde{i}_b \\
\dot{\hat{\xi}}_b &= -Ri_b + u_b + \gamma_\theta\left(\hat{\xi}_b - Li_b\right)\mathcal{F} + \frac{p\hat{\omega}}{L\gamma_1}\tilde{i}_a.
\end{aligned}
\tag{11}
$$

When no stator current estimation laws are implemented in Observer I [with the γ_1-dependent terms in $\dot{\hat{\xi}}_a$ and $\dot{\hat{\xi}}_b$ being accordingly set to zero and the observer (7)-(8) exactly reducing to the one in [24] and [27]], the resulting modification leading to the scheme of Figure 3 just consists of including the torque estimation law in the speed tracking control loop and of replacing the speed estimate provided by (4) of [24] by the corresponding one provided by the PLL-SSLKF block.

B. Modified Observer II

The modified Observer II naturally reads (k_i, k_E are positive design parameters):

$$
\begin{aligned}
\frac{d\hat{i}_a}{dt} &= -\frac{R}{L}i_a + \frac{k_M}{L}\hat{\omega}\widehat{\sin(p\theta)} + \frac{u_a}{L} + k_i(i_a - \hat{i}_a) \\
\frac{d\hat{i}_b}{dt} &= -\frac{R}{L}i_b - \frac{k_M}{L}\hat{\omega}\widehat{\cos(p\theta)} + \frac{u_b}{L} + k_i(i_b - \hat{i}_b) \\
\frac{d\widehat{\cos(p\theta)}}{dt} &= -p\hat{\omega}\widehat{\sin(p\theta)} + v_c \\
\frac{d\widehat{\sin(p\theta)}}{dt} &= p\hat{\omega}\widehat{\cos(p\theta)} + v_s \\
v_c &= -k_E\hat{\omega}(i_b - \hat{i}_b) \\
v_s &= k_E\hat{\omega}(i_a - \hat{i}_a).
\end{aligned}
\tag{12}
$$

VI. Experimental Set-up

The prototype realization of the electric drive shown in Figure 4 and Figure 5 is used to experimentally investigate the effectiveness of the proposed modified observers to be included into the sensorless control algorithm of Figure 3. The control board sits on top of the inverter and it is connected by a high density flat cable to the gate drivers and sensors. The electrical drive is fully controlled by the National Instruments System-on-Module sbRIO-9651, with a dedicated board specifically designed for power electronics and drives applications (PED-Board®). The proposed observers are directly implemented, in their discrete-time versions (execution time $T_e = 83$ μs), on the FPGA target using a 32-bit floating point arithmetic. In the test campaign, an axial flux, permanent magnets, 5 pole-pairs machine (35 kW, 3000 rpm, 110 A, $L = 0.000036$ H, $R = 0.1$ Ω, $J = 0.5$ kg m^2, $k_M = 1.14$ N m A^{-1}) is used with a constant reference speed equal to 250 rpm and a $|0.875|$ N m -torque. The 1 ppr sensor is emulated by updating only once per

round the speed measurement provided by a resolver having 30 rpm resolution. The phase voltage values applied to the PMSM are assumed to coincide with the reference voltages provided as inputs to the PWM modulator and thus they are not physically measured. To perform the tuning of PLL-SSLKF parameters, the practical off-line procedure proposed in [37] has been accounted with $\omega_n = 20$, $R = 2$ and $\phi = 45$ degree.
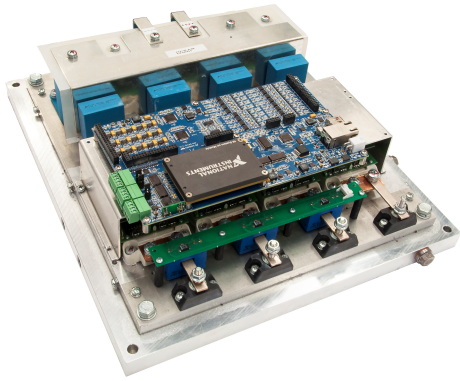

Fig. 4. FPGA controlled 3-ph inverter prototype used in the experimental campaign.

Fig. 5. Detailed view of the axial-flux PM-machine at the test bed.

VII. EXPERIMENTAL RESULTS

In this section experimental results showing the effectiveness of the proposed PLL-SSLKF-based sensorless control are provided in a speed sensor fault-tolerant scenario[2]. The design parameters (in SI units) are: $k_e = 15000$, $\gamma_\theta = 2000$, $\gamma_1 = 1000$ for Observer I; $k_i = 2000$, $k_E = 20$ for Observer II. The motor is initially controlled, to reach the steady-state, by the standard field oriented controller (6) with the measured speed ω in place of estimated one $\hat\omega$ and with the measurements of $\sin(p\theta)$, $\cos(p\theta)$ in place of the estimated ones $\widehat{\sin(p\theta)}_f$, $\widehat{\cos(p\theta)}_f$ [no related Figures are included for

[2]We here assume, for the sake of simplicity, that a speed sensor fault detection scheme is available.

the sake of brevity]. The control parameters [in SI units]: $k_\omega = 0.01$, $k_{\omega I} = 0.004$, $k_i = 0.0101022$, $k_{iI} = 3.6538$ have been set by adopting the tuning techniques of [72] relying on the Bode diagrams for the speed/current control loops.

A. Sensorless control of Figure 3 (steady-state)

The sensorless control of this paper is activated at time $t = 0$. Figures 6-10 illustrate the closed loop performance obtained by the PLL-SSLKF-based sensorless control of Figure 3 including the modified Observers I and II. Satisfactory results are achieved in both cases: rather precise speed regulation is guaranteed, along with small estimation errors for $\sin(p\theta)$, $\cos(p\theta)$ and small tracking errors for the (i_d, i_q)- tracking errors. An improved performance is, however, obtained in the case of the modified (global) Observer II.
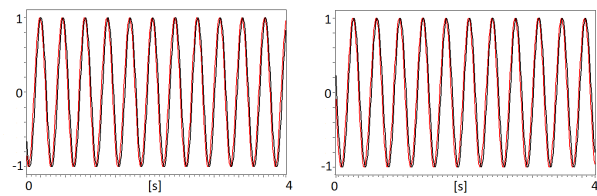

Fig. 6. Experiments of Subsection A. Estimated $\cos(p\theta)$ (i.e., $\widehat{\cos(p\theta)}_f$) for the modified Observers I (left subplot) and II (right subplot), in comparison with the corresponding actual profiles.
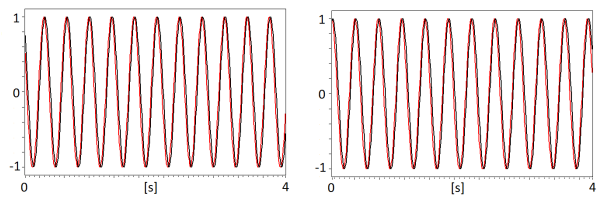

Fig. 7. Experiments of Subsection A. Estimated $\sin(p\theta)$ (i.e., $\widehat{\sin(p\theta)}_f$) for the modified Observers I (left subplot) and II (right subplot), in comparison with the corresponding actual profiles.
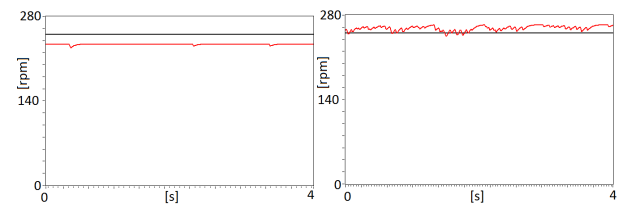

Fig. 8. Experiments of Subsection A. Rotor speed and rotoor speed reference for the sensorless control with the modified Observers I (left subplot) and II (right subplot).

B. Position-sensorless control of Figure 1 (steady-state)

As comparison, the experimental results (at steady-state) obtained by the position-sensorless control of Figure 1 in [30], which is activated at time $t = 0$ and relies on 1 ppr speed sensor-based measurements, are reported. The same design parameters of the corresponding sensorless
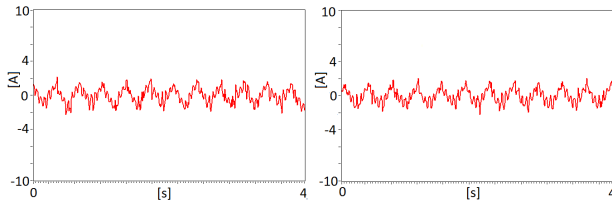
Fig. 9. Experiments of Subsection A. i_d-current tracking error for the sensorless control with the modified Observers I (left subplot) and II (right subplot).
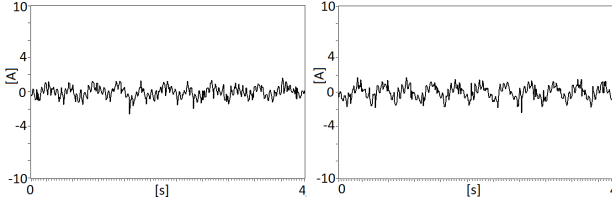

Fig. 10. Experiments of Subsection A. i_q-current tracking error for the sensorless control with the modified Observers I (left subplot) and II (right subplot).

scenario are used. Figures 11-13 illustrate the closed loop performance. Even though more precise position estimation and speed regulation are achieved in the presence of speed information, the closed loop performance is not so far from the one achieved in the previous sensorless scenario (slightly improved performance is again obtained in the case of the Observer II). Such results definitely confirm the effectiveness of the sensorless approach of this paper, but they also explicitly confirm, from an experimental point of view, the ideas described in [30].
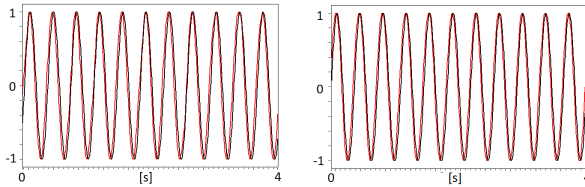

Fig. 11. Experiments of Subsection B. Estimated $\cos(p\theta)$ (i.e., $\widehat{\cos(p\theta)}_f$) for Observers I and II in [30], in comparison with the corresponding actual profiles.
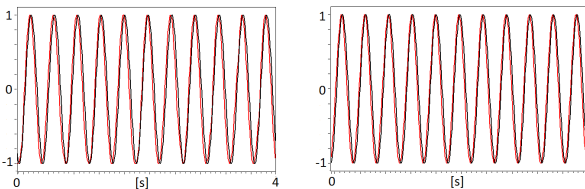

Fig. 12. Experiments of Subsection B. Estimated $\sin(p\theta)$ (i.e., $\widehat{\sin(p\theta)}_f$) for Observers I and II in [30], in comparison with the corresponding actual profiles.

C. Sensorless control of Figure 3 (transient)

The sensorless control of Figure 3, incorporating Observer II, is activated at time $t = 0$. The speed reference is abruptly
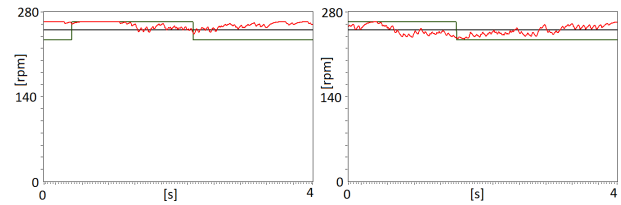

Fig. 13. Experiments of Subsection B. Rotor speed and its reference, along with the rotor speed measured through the 1 ppr-sensor (dark green), for Observers I and II in [30].

modified after $t = 1$ s. Figure 14 illustrates the closed loop performance in two cases: i) speed reference passing from 350 rpm to 250 rpm; ii) speed reference passing from 250 rpm to 350 rpm. The time profile of the estimated speed is reported in both cases, along with the time profile of the time-varying speed reference. In both cases, the estimated speed exhibits a smooth profile reaching, with acceptable oscillations, the new steady-state value after about 1 s.
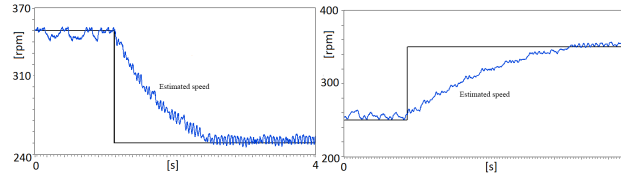

Fig. 14. Experiments of Subsection C. Rotor speed estimate and its reference for the sensorless control of Figure 3 with Observer II.

D. Transition from the position-sensorless control of Figure 1 to the sensorless control of Figure 3

The position-sensorless control of Figure 1, relying on 1 ppr speed sensor-based measurements, is activated at time $t = 0$. A complete speed sensor fault occurs before the time instant $t = 2$ s, with the corresponding sensorless control of Figure 3 being simultaneously activated. Figure 15 illustrates the smooth transition between the two controls of Figure 1 and 3. Satisfactory results are achieved: rather precise speed regulation is guaranteed *pre-* and *post-* fault. An improved performance is again obtained in the case of the control scheme incorporating Observer II.
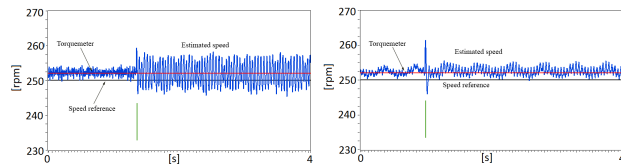
Fig. 15. Experiments of Subsection D. Transition from the position-sensorless control (Figure 1) to the sensorless control (Figure 3): (torque-meter measured) rotor speed and its reference, along with the rotor speed measured through the 1 ppr-sensor and the estimated speed, for Observers I and II and modified Observers I and II.

VIII. CONCLUSIONS

Effective 'minimum distance' adaptations of the latest position-sensorless design ideas have led to new sensorless

observers to be included into a simple adaptive observer-based sensorless speed control for (nonsalient-pole surface) PMSMs. Such a sensorless control scheme owns a definite flavour inherited from the electric machines control literature. The underlying idea has been to replace the measured rotor speed of the position-sensorless control with the estimated speed that is provided by the third-order PLL-SSLKF being already used, in the position-sensorless control, to mitigate the distortions on the estimated position. Experimental results have demonstrated, in terms of steady-state/transient behaviours and *pre/post* fault transition, the effectiveness of the proposed approach in a speed sensor fault-tolerant scenario.

REFERENCES

[1] M. Bodson, J.N. Chiasson, R.T. Novotnak, R.B. Rekowski. High-performance nonlinear feedback control of a permanent magnet stepper motor. *IEEE Transactions on Control Systems Technology*, 1: 5-14, 1993.

[2] J. Chiasson. *Modeling and High-Performance Control of Electric Machines*. Wiley-IEEE Press: Hoboken, 2005.

[3] D.M. Dawson, J. Hu, T.C. Burg. *Nonlinear Control of Electric Machinery*. Marcel Dekker: New York, 1998.

[4] S. Di Gennaro. Adaptive output feedback control of synchronous motors. *International Journal of Control*, 73: 1475-1490, 2000.

[5] F. Khorrami, P. Krishnamurthy, H. Melkote. *Modeling and Adaptive Nonlinear Control of Electric Motors*. Springer-Verlag: Berlin, 2003.

[6] R. Marino, S. Peresada, P. Tomei. Nonlinear adaptive control of permanent magnet step motors. *Automatica*, 31: 1595-1604, 1995.

[7] M. Zribi, J.N. Chiasson. Position control of a PM stepper motor by exact linearization. *IEEE Transactions on Automatic Control*, 36: 620-625, 1991.

[8] Z. Ping, J. Huang. Speed tracking control of surface-mounted permanent-magnet synchronous motor with unknown exosystem. *International Journal of Robust and Nonlinear Control*, 25: 1247-1264, 2015.

[9] C.M. Verrelli. Fourier series expansion for synchronization of permanent magnet electric motors. *Applied Mathematics and Computation*, 217: 4502-4515, 2011.

[10] C.M. Verrelli. Synchronization of permanent magnet electric motors: new nonlinear advanced results. *Nonlinear Analysis: Real World Applications*, 13: 395-409, 2012.

[11] C.M. Verrelli, S. Pirozzi, P. Tomei, C. Natale, S. Bifaretti, A. Lidozzi, M. Tiberti, D. Diaferia. Synchronization control of electric motors through adaptive disturbance cancellation. *International Journal of Control*, http://dx.doi.org/10.1080/00207179.2016.1222556.

[12] V. Salis, N. Chiappinelli, A. Costabeber, P. Zanchetta, S. Bifaretti, P. Tomei, C.M. Verrelli. Learning position controls for hybrid step motors: from current-fed to full-order models. *IEEE Transactions on Industrial Electronics*, 65: 6120-6130, 2018.

[13] C.M. Verrelli, P. Tomei, L. Consolini, E. Lorenzani. Space-learning tracking control for permanent magnet motors. *Automatica*, 73: 223-230, 2016.

[14] S. Bifaretti, V. Iacovone, A. Rocchi, P. Tomei, C.M. Verrelli. Nonlinear speed tracking control for sensorless PMSMs with unknown load torque: from theory to practice. *Control Engineering Practice*, 20: 714-724, 2012.

[15] G. Bisheimer, M.O. Sonnaillon, C.H. De Angelo, J.A. Solsona, G.O. García. Full speed range permanent magnet synchronous motor control without mechanical sensors. *IET Electric Power Applications*, 4: 35-44, 2010.

[16] T.F. Chan, W. Wang, P. Borsje, Y.K.Wong, S.L. Ho. Sensorless permanent-magnet synchronous motor drive using a reduced-order rotor flux observer. *IET Electric Power Applications*, 2: 88-98, 2008.

[17] C. De Angelo, G. Bossio, J. Solsona, G.O. García, M.I. Valla. Mechanical sensorless speed control of permanent-magnet AC motors driving an unknown load. *IEEE Transactions on Industrial Electronics*, 53: 406-414, 2006.

[18] M. Hinkkanen, T. Tuovinen, L. Harnefors, J. Luomi. A combined position and stator-resistance observer for salient PMSM drives: design and stability analysis. *IEEE Transactions on Power Electronics*, 27: 601-609, 2012.

[19] B. Nahid-Mobarakeh, F. Meibody-Tabar, F.M. Sargos. Back EMF estimation-based sensorless control of PMSM: robustness with respect to measurement errors and inverter irregularities. *IEEE Transactions on Industrial Electronics*, 43: 485-494, 2007.

[20] M. Rashed, P.F.A. MacConnell, A.F. Stronach, P. Acarnley. Sensorless indirect-rotor-field-orientation speed control of a permanent-magnet synchronous motor with stator-resistance estimation. *IEEE Transactions on Industrial Electronics*, 54: 1664-1675, 2007.

[21] M. Seilmeier, B. Piepenbreier. Sensorless control of PMSM for the whole speed range using two-degree-of-freedom current control and HF test current injection for low-speed range. *IEEE Transactions on Power Electronics*, 30: 4394-4403, 2015.

[22] D. Shah, G. Espinosa-Pérez, R. Ortega, M. Hilairet. An asymptotically stable sensorless speed controller for non-salient permanent magnet synchronous motors. *International Journal of Robust and Nonlinear Control*, 24: 644-668, 2014.

[23] P. Tomei, C.M. Verrelli. A nonlinear adaptive speed tracking control for sensorless permanent magnet step motors with unknown load torque. *International Journal of Adaptive Control and Signal Processing*, 22: 266-288, 2008.

[24] P. Tomei, C.M. Verrelli. Observer-based speed tracking control for sensorless permanent magnet synchronous motors with unknown load torque. *IEEE Transactions on Automatic Control*, 56: 1484-1488, 2011.

[25] C.M. Verrelli, P. Tomei, E. Lorenzani, G. Migliazza, F. Immovilli. Nonlinear tracking control for sensorless permanent magnet synchronous motors with uncertainties, *Control Engineering Practice*, 60: 157-170, 2017.

[26] J. Lee, J. Hong, K. Nam, R. Ortega, L. Praly, A. Astolfi. Sensorless control of surface-mount permanent magnet synchronous motors based on a nonlinear observer. *IEEE Transactions on Power Electronics*, 25: 290-297, 2010.

[27] R. Ortega, L. Praly, A. Astolfi, J. Lee, K. Nam. Estimation of rotor position and speed of permanent magnet synchronous motors with guaranteed stability, *IEEE Transactions on Control Systems Technology*, 19: 601-614, 2011.

[28] A. Tilli, G. Cignali, C. Conficoni, C. Rossi. A synchronous coordinates approach in position and speed estimation for permanent magnet synchronous machines. *2012 20th Mediterranean Conference on Control & Automation*, 487-492, Barcelona, Spain, 3-6 July, 2012.

[29] A. Tilli, C. Conficoni, G. Cignali. Globally asymptotically stable reconstruction of flux, rotor position and speed for permanent magnets machines. *2014 22nd Mediterranean Conference on Control & Automation*, 1211-1216, Palermo, Italy, June 16-19, 2014.

[30] S. Bifaretti, A. Lidozzi, L. Solero, M. Tiberti, P. Tomei, C.M. Verrelli. Position estimation for permanent magnets synchronous machines in pump-fan and generating applications. *7th IEEE International Symposium on Sensorless Control of Electrical Drives (SLED 2016)*, 1-6, Dinarau, Nadi, FIJI, June 5-6, 2016.

[31] C.M. Verrelli, P. Tomei, E. Lorenzani. Persistency of excitation and position-sensorless control of permanent magnet synchronous motors. *Automatica*, 95: 328-335, 2018.

[32] J.G. Romero, R. Ortega, Z. Han, T. Devos, F. Malrait. An adaptive flux observer for the permanent magnet synchronous motor. *International Journal of Adaptive Control and Signal Processing*, 30: 473-487, 2016.

[33] R. Marino, P. Tomei, C.M. Verrelli. Adaptive output-feedback control of induction motors. Chapter of Book in *AC Electric Motors Control: Advanced Design Techniques and Applications*. Wiley-Blackwell, 2013.

[34] P. Tomei, C.M. Verrelli. Advances on adaptive learning control: the case of non-minimum phase linear systems, *Systems and Control Letters*, 115: 55-62, 2018.

[35] Z. Zhang, C. Hackl, F. Wang, Z. Chen, R. Kennel. Encoderless model predictive control of back-to-back converter direct-drive permanent-magnet synchronous generator wind turbine systems. *Proceedings of the 15th European Conference on Power Electronics and Applications (EPE)*, 1-10, Lille (France), September 3-5, 2013.

[36] A. Bellini, S. Bifaretti. Performances of a PLL based digital filter for double-conversion UPS. *Proceedings of the 13th International Conference on Power Electronics and Motion Control, EPE-PEMC 2008*, 490-497, Poznan (Poland), September 1-3, 2008.

[37] S. Bifaretti, P. Zanchetta, E. Lavopa. Comparison of two three-phase PLL systems for more electric aircraft converters. *IEEE Transactions on Power Electronics*, 29: 6810-6820, 2014.

[38] M. Abdelrahem, A.E. Hafni, R. Kennel, C.M. Hackl. Predictive Phase Locked loop for sensorless control of PMSG based variable-speed wind turbines. *2017 IEEE 8th International Symposium on Sensorless Control for Electrical Drives (SLED 2017)*, 151-156, Catania, Italy, September 18-19, 2017.

[39] A. Bellini, S. Bifaretti. A digital filter for speed noise reduction in drives using an electromagnetic resolver. *Mathematics and Computers in Simulation*, 71: 476-486, 2006.

[40] A. Bellini, S. Bifaretti, S. Costantini. A digital speed filter for motion control drives with a low resolution position encoder. *Automatika*, 44: 6774, 2003.

[41] J. Lara, A. Chandra. Performance investigation of two novel HSFSI demodulation algorithms for encoderless FOC of PMSMs intended for EV propulsion. *IEEE Transactions on Industrial Electronics*, 65: 1074-1083, 2018.

[42] M. Abdelrahem, C.M. Hackl, Z. Zhang, R. Kennel. Robust predictive control for direct-driven surface-mounted permanent-magnet synchronous generators without mechanical sensors. *IEEE Transactions on Energy Conversion*, 33: 179-189, 2018.

[43] R. Morales-Caporal, E. Bonilla-Huerta, C. Hernández, M.A. Arjona, M. Pacas. Transducerless acquisition of the rotor position for predictive torque controlled PM synchronous machines based on a DSP-FPGA digital system. *IEEE Transactions on Industrial Informatics*, 9: 799-807, 2013.

[44] M. Abdelrahem, P. Catterfeld, C.M. Hackl, R. Kennel. A sliding-mode-observer for encoderless direct model predictive control of PMSGs. *PCIM 2018*, 1257-1264, Nuremberg, Germany, June 5-7, 2018.

[45] I. Boldea, S.A. Nasar, *Electrical Drives*, CRC Press, 2017.

[46] C.M. Verrelli, E. Lorenzani, R. Fornari, M. Mengoni, L. Zarri. Steady-state speed sensor fault detection in induction motors with uncertain parameters: A matter of algebraic equations. *Control Engineering Practice*, 80: 125-137, 2018.

[47] M. Riera-Guasp, J.A. Antonino-Daviu, G.A. Capolino. Advances in electrical machine, power electronic, and drive condition monitoring and fault detection: state of the art. *IEEE Transactions on Industrial Electronics*, 62: 1746-1759, 2015.

[48] M.O. Mustafa, G. Nikolakopoulos, T. Gustafsson, D. Kominiak. A fault detection scheme based on minimum identified uncertainty bounds violation for broken bars in induction motors. *Control Engineering Practice*, 48: 6-77, 2016.

[49] M.O. Mustafa, D. Varagnolo, G. Nikolakopoulos, T. Gustafsson. Detecting broken rotor bars in induction motors with model-based support vector classifiers. *Control Engineering Practice*, 52: 15-23, 2016.

[50] I. Martin-Diaz, D. Morinigo-Sotelo, O. Duque-Perez, R. de J. Romero-Troncoso. Early fault detection in induction motors using AdaBoost with imbalanced small data and optimized sampling. *IEEE Transactions on Industry Applications*, 53: 3066-3075.

[51] A. Giantomassi, F. Ferracuti, S. Iarlori, G. Ippoliti, S. Longhi. Electric motor fault detection and diagnosis by Kernel density estimation and Kullback-Leibler divergence based on stator current measurements. *IEEE Transactions on Industrial Electronics*, 62: 1770-1780, 2015.

[52] C. Chakraborty, V. Verma. Speed and current sensor fault detection and isolation technique for induction motor drive using axes transformation. *IEEE Transactions on Industrial Electronics*, 62: 1943-1954, 2015.

[53] H. Alwi, C. Edwards. Development and application of sliding mode LPV fault reconstruction schemes for the ADDSAFE benchmark. *Control Engineering Practice*, 31: 148-170, 2014.

[54] J. Guzinski, H. Abu-Rub, M. Diguet, Z. Krzeminski, A. Lewicki. Speed and load torque observer application in high-speed train electric drive. *IEEE Transactions on Industrial Electronics*, 57: 565-574, 2010.

[55] S.K. Kommuri, J.J. Rath, K.C. Veluvolu, M. Defoort, Y.C. Soh. Decoupled current control and sensor fault detection with second-order sliding mode for induction motor. *IET Control Theory and Applications*, 9: 608-617, 2015.

[56] A. Raisemche, M. Boukhnifer, C. Larouci, D. Diallo. Two active fault-tolerant control schemes of induction-motor drive in EV or HEV. *IEEE Transactions on Vehicular Technology*, 63: 19-29, 2014.

[57] M.E.H. Benbouzid, D. Diallo, M. Zeraoulia. Advanced fault-tolerant control of induction-motor drives for EV/HEV traction applications: from conventional to modern and intelligent control techniques. *IEEE Transactions on Vehicular Technology*, 56: 519-528, 2007.

[58] F. Aguilera, P.M. de la Barrera, C.H. De Angelo, D.R. Espinoza Trejo. Current-sensor fault detection and isolation for induction-motor drives using a geometric approach. *Control Engineering Practice*, 53: 35-46, 2016.

[59] D.U. Campos-Delgado, D.R. Espinoza-Trejo, E. Palacios. Fault-tolerant control in variable speed drives: a survey. *IET Electric Power Applications*, 2: 121-134, 2008.

[60] T.A. Najafabadi, F.R. Salmasi, P. Jabehdar-Maralani. Detection and isolation of speed-, DC-link voltage-, and current-sensor faults based on an adaptive observer in induction-motor drives. *IEEE Transactions on Industrial Electronics*, 58: 1662-1672, 2011.

[61] B. Tabbache, M. Benbouzid, A. Kheloui, J.-M. Bourgeot. A fuzzy-based strategy to improve control reconfiguration performance of a sensor fault-tolerant induction motor propulsion. *International Review on Modelling and Simulation*, 4: 1168-1171, 2011.

[62] J. Guzinski, M. Diguet, Z. Krzeminski, A. Lewicki, H. Abu-Rub. Application of speed and load torque observers in high-speed train drive for diagnostic purposes. *IEEE Transactions on Industrial Electronics*, 56: 248-256, 2009.

[63] F. Zidani, D. Diallo, M.E.H. Benbouzid, E. Berthelot. Diagnosis of speed sensor failure in induction motor drive. *IEEE International Electric Machines & Drives Conference*, 2: 1680-1684, May 3-5 2007.

[64] S.M. Bennet, R.J. Patton, S. Daley. Sensor fault-tolerant control of a rail traction drive. *Control Engineering Practice*, 7, 217-225, 1999.

[65] D. Diallo, M.E.H. Benbouzid, A. Makouf. A fault-tolerant control architecture for induction motor drives in automotive applications. *IEEE Transactions on Vehicular Technology*, 53: 1847-1855, 2004.

[66] K.-S. Lee, J.-S. Ryu. Instrument fault detection and compensation scheme for direct torque controlled induction motor drives. *IEE Proceedings on Control Theory and Applications*, 150: 376-382. 2003.

[67] M.E. Romero, M.M. Seron. Speed-sensorless control of induction motors with improved fault tolerance against current sensor failure. *18th Mediterranean Conference on Control & Automation*, 515-520, June 23-25 2010.

[68] M.E. Romero, M.M. Seron, J.A. De Doná. Sensor fault-tolerant vector control of induction motors. *IET Control Theory and Applications*, 4: 1707-1724, 2010.

[69] H. Wang, S. Pekarek, B. Fahimi. Multilayer control of an induction motor drive: a strategic step for automotive applications. *IEEE Transactions on Power Electronics*, 21: 676-686, 2006.

[70] C.M. Verrelli, S. Bifaretti, A. Lidozzi, L. Solero, F. Crescimbini. Sensorless control for PM-machine based generating units. *2017 IEEE 8th International Symposium on Sensorless Control for Electrical Drives (SLED 2017)*, 231-236, Catania, Italy, September 18-19, 2017.

[71] H.K. Khalil. *Nonlinear Systems*. Prentice Hall: Upper Saddle River, 2002.

[72] A. Lidozzi, V. Serrao, L. Solero, F. Crescimbini, A. Di Napoli. Direct tuning strategy for PMSM drives. *2008 IEEE Industry Applications Society Annual Meeting*, 1-7, Edmonton, AB, Canada, October 5-9, 2008.